Journal of Materials Chemistry A

Accepted Manuscript

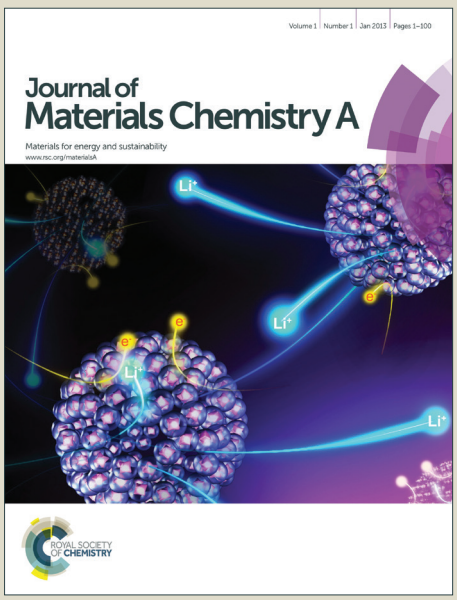

ROYAL SOCIETY OF CHEMISTRY

www.rsc.org/materialsA

Graphical abstract

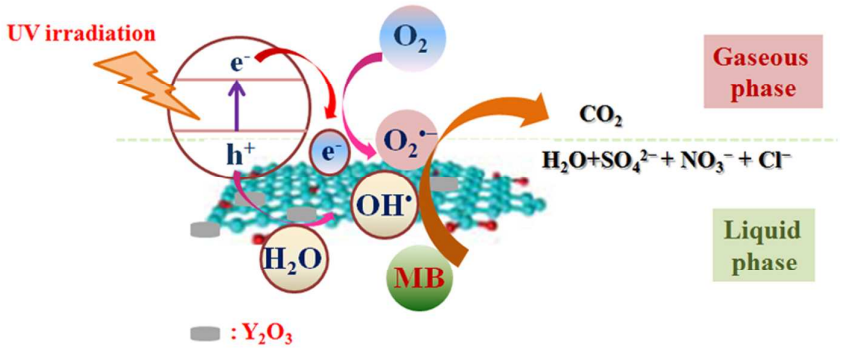

A novel yttrium-doped graphene oxide (GOY) composite was firstly prepared and its photocatalytic performance was investigated by degradation of MB.

Synthesis of novel Yttrium-doped graphene oxide nanocomposite for dye removal

Ya Zhang[1*], Saisai Yuan[2], Yanhua Zhao[1], Honggui Wang[1], Chenda He[1*]

1. Jiangsu Key Laboratory of Environmental Material and Engineering, School of Environmental Science and Engineering, Yangzhou University, Yangzhou, 225127, P.R. China.

2. School of Chemistry and Chemical Engineering, Yangzhou University, Yangzhou, 225009, P.R. China

ABSTRACT:

A novel yttrium-doped graphene oxide (GOY) composite was prepared by hydrothermal method. The morphology results showed that the graphene oxide (GO) can successfully composite with yttrium and the as-prepared GOY had a nanoflake structure. From the photoelectrochemical analysis and photoluminescence (PL) spectra, the primary role of GO in Y_2O_3 was confirmed as an electron conductor, enhancing the photocurrent density. As expected, the as-obtained GOY composites had better photocatalytic performance on decomposition of methylene blue molecules than bare GO and Y_2O_3. The 5 GOY (10 mg) could degrade MB (25 ppm) thoroughly (~100 %) within 10 min, which was quite comparable with the commercial TiO_2 P25 under UV irradiation. A possible mechanism of photocatalysis was also been presented.

Keywords: Yttrium-doped graphene oxide, Methylene blue, Ultraviolet light, Photocatalyst.

1. Introduction

Nowadays, the growing population has led to the increasing contamination of surface and ground water. Organic dyes used in textile and food industries are one of the important sources of the environmental contaminations due to their non-biodegradability and high toxicity to aquatic creatures and carcinogenic effects on humans.[1,2] Semiconductor photocatalysis has been extensively studied as a viable water treatment method.[3,4] Photocatalyst, which accelerates light-driven chemical reactions, has been paid a great

* Corresponding author. Tel: +86-514-87979528; E-mail address: zhangya@yzu.edu.cn (Y. Zhang), hcd@yzu.edu.cn (C.D. He).

attention due to fascinating properties such as quantum confinement and enhanced reactivity.[5] Up to date, diverse photocatalytic materials have been introduced, including TiO_2, ZnO, Fe_3O_4, SnO_2, and $BiVO_4$.[3, 6-10] Graphene oxide (GO), a two-dimensional sheet of sp^2 hybridized carbon composing of only carbon, oxygen, and hydrogen, has a high specific surface area and tunable electronic structure.[11–13] Due to its extraordinary physical properties, high chemical and thermal stability, graphene has been receiving recent attention as a support for catalysts.[13-15] Recently, a TiO_2 nanorod-decorated graphene sheets has been prepared by Jang and coworkers.[14] This nanocomposite had highly efficient photocatalytic activities under visible-light irradiation. Wang et al., has reported a high-performance and recyclable visible-light photocatalysis, cobalt ferrite and graphene composite.[15] The spontaneous exfoliated GO as an auxiliary co-catalyst has been reported that it can remarkably enhanced the photocatalytic hydrogen production of TiO_2.[16] Although graphene has shown potential applications in water treatment as a photocatalyst, further optimization or modification of the GO structure is still necessary for enhancing its photocatalytic activity.

Impurity doping with proper oxidation state is useful for red shifting the absorption edge as well as reducing the rate of electron-hole pair's recombination which improves the photocatalytic activity of a photocatalyst.[4,17,18] It is reported that yttrium doping in TiO_2 gives improved photocatalytic response attributed to the visible light absorption, electron-hole pair's separation, higher interfacial charge transfer, lower crystallite size and high specific surface area.[4,19-21] This property enhances the performance of Y-based catalysts used in wastewater treatment.

In this work, a novel yttrium-doped GO (GOY) was firstly synthesized via hydrothermal method with different GO doping concentration. The as-synthesized samples were characterized by XRD, FT-IR, FESEM, HRTEM and XPS. The corresponding photocatalytic activity was evaluated by measuring the photocatalytic degradation of methylene blue (MB) and methlene orange (MO) degradation under UV irradiation. A possible mechanism of photocatalysis was also been presented based on the results of photoelectrochemical analysis and PL spectra.

2. Experimental

Yttrium (III) nitrate hexahydrate ($Y(NO_3)_3 \cdot 6H_2O$), polyvinylpyrrolidone ($(C_6H_9NO)_n$), ethanol, graphite, NaCl, H_2SO_4, H_2O_2, P_2O_5 and $K_2S_2O_7$ were purchased from Sinopharm Chemical Reagent Company. TiO_2 P25 was obtained from Evonik Industries. All the reagents were of analytical grade and used as received without further treatment. All solutions were prepared with DI water.

2.1. Preparation of Y_2O_3 and GO/ Y_2O_3 composite catalysts

GO was prepared via a modified Hummer method as reported previously.[22] In a typical synthesis procedure, 0.776 g Yttrium (III) nitrate hexahydrate ($Y(NO_3)_3 \cdot 6H_2O$), 0.223g polyvinylpyrrolidone ($(C_6H_9NO)_n$) and certain amounts of GO were dissolved in a 7 mL DI water and 33 mL ethanol. Then the solution dissolved under magnetic stirring. The obtained transparent solution was transferred into a 50 mL polytetrafluoroethylene (PTFE) (Teflon)-lined steel autoclaves and heated at 180 ^oC for 16 h. After cooling to ambient temperature, the precipitate was centrifuged, washed several times with ethanol, and dried at 60 ^oC in an oven. As a control experiment, Y_2O_3 nanoparticles were prepared under the same conditions without adding GO. The Y-doped GO composite containing 5, 10, 20 and 50 mg GO are denoted as 5 GOY, 10 GOY, 20 GOY and 50 GOY, respectively.

2.2. Characterization

The X-ray diffraction (XRD) patterns were obtained by a Bruker D8 advance X-ray diffractometer using monochromatic Cu Kα radiation (λ = 1.5406 Å) with an accelerating voltage of 40 kV and current of 40 mA. The 2θ range used in the measurement was from 10 to 70◦. The FT-IR spectra of the samples were measured on a Cary 610/670 microscope (Varian, US), with scanning from 4000 to 400 cm^{-1} by using KBr pellets under ambient temperature. Thermogravimetric analysis (TGA) was performed with a PE Pyris-1 instrument at a heating rate of 10 ^oC min^{-1} under N_2 atmosphere. Field emission scanning electron microscopy (FESEM) was examined on a field-emission scanning electron microanalyzer (Hitachi S-4800, Japan). Energy dispersive X-ray spectroscopy (EDX) was performed on a XL-30ESEM scanning electron microscopy. High-resolution transmission electron microscopy (HRTEM) was recorded on a Tecnai G2 F30 S-TWIN transmission electron microscopes. X-ray photoelectron spectroscopy (XPS) measurements were carried out with

an ESCALAB 250 photoelectron spectrometer using Al Kα radiation (Thermo-VG Scientific, US). The photoluminescence (PL) spectra were measured with a JY HRD double grating monochromator at room temperature.

2.3. Degradation of methylene blue (MB) and methylene orange (MO)

Photocatalysis experiments were carried out in a BL-GHX-V photochemical reactor (Shanghai Bilon Instrument Co., Ltd). The UV source ($\lambda < 420$ nm) was provided by a 500 W high-pressure mercury lamp. Reactor and UV source were surrounded by a circulating water jacket to maintain constant temperature. UV irradiation photocatalytic activities of GO, Y_2O_3 and GOY composite were evaluated through the degradation of MB and MO.

A stock solution of MB (or MO) at 1000 ppm was prepared using DI water. In a typical run, 0.05 g of photocatalyst was dispersed in a 20 mL MB (or MO) (25 ppm). Then the suspension was stirred for 30 min in the dark to ensure adsorption/desorption equilibrium before light illumination. At each specific sampling time, aqueous sample was withdrawn by a 5 mL syringe, and filtered immediately by a 0.22 μm filter film to remove the catalyst particles before analysis. All experiments were repeated at least two times, and averages were reported. The concentration of MB (or MO) was then determined by measuring the absorbance at λ_{max} 600 nm via UV-vis spectrophotometer. To determine the catalytic recycling properties, the catalyst was separated after reaction for 30 min, and washed thoroughly with ultrapure water and ethanol, followed by drying at 60 ^{o}C for 12 h in vacuum oven. Finally, the catalyst was separated by magnet and redispersed in a new reaction system for subsequent catalytic experiments under the same reaction conditions. The reduction ratio of MB (or MO) was calculated using the following expression:

$$\text{Degradation ratio of MB} = \frac{(A_0 - A_t)}{A_0} \times 100\%$$

where A_0 and A_t were the absorbance intensities when illuminated for 0 (that is, just after the dark adsorption) and t min, respectively.

2.4. Photoelectrochemical Measurements

All photoelectrochemical characteristics were performed in the electrolytic cell consisted of a GO, Y_2O_3 or GOY composites (2 mg mL^{-1}, 100 μL) coated FTO glass working electrode (2cm*2cm), a platinum wire counter electrode and a saturated calomel reference

electrode (SCE) on a Model CHI 660E electrochemical workstation under a 500 W high-pressure mercury lamp irradiation.

3. Results and discussion

3.1. FT-IR spectra, XRD and TGA Analysis .

FT-IR measurement is employed to investigate the bonding interactions in GO before and after the oxidation process. FT-IR spectra of GO, Y_2O_3 and 5 GOY are shown in Fig. 1. In the spectrum of GO, the peak at about 1721 cm^{-1} is attributed to the stretching vibrations of C=O. The peaks appear at about 1223 and 1564 cm^{-1} correspond to the stretching vibrations of C-O and C=C, respectively.[23] The FT-IR spectra of Y_2O_3 and 5 GOY composite have similar curve shape, while a new peak appears at 1550 cm^{-1} of 5 GOY. This result indicates the GO has successfully composited with Y_2O_3.

Fig. 2 shows the crystal structure of GO, Y_2O_3 and 5 GOY composite. GO shows a sharp peak at $2\theta = 10.5^{o}$, corresponding to the (001) reflection of graphite oxide.[15,24,25] The diffraction peaks observed at $2\theta = 42.1°$ originate from disorderedly stacked GO sheets.[26] The peaks located at 19.8°, 28.6°, 35.1°, 50.1°, 49.4° and 51.2° (2θ) result from the presence of Y_2O_3, which are in agreement with the theoretical data of hematite (JCPDS No: 41-0015).[27,28] In the pattern of 5 GOY, the presence of diffraction peak at 2θ of 42.1° indicating that GO exists in the composite material. It should be noted that there is a diffraction peak observed at $2\theta = 10.1°$ on both patterns of Y_2O_3 and 5 GOY, which originates from intermediate YO(OH) structure.[27]

Fig. 3 presents results of TGA analysis of the as-synthesized GO, Y_2O_3 and 5 GOY composite powder. The samples were heated from room temperature to 600 °C at 5 °C min^{-1} under N_2 flow. As can be seen in Fig.3, GO starts to lose mass upon heating even below 100 °C. The major mass loss occurs at about 200 °C is caused by pyrolysis of the oxygen-containing functional groups, generating CO, CO_2 and stream.[29-31] Y_2O_3 and 5 GOY have the same shape and show mass losses at three temperature ~100, 320 and 400 °C. The first mass loss at about 100 °C is related to dehydration of free and physically absorbed molecular water. The next mass loss at about 320 °C is supposed to be related with the first dehydration of chemisorbed and combined water from $Y(OH)_3$.[32,33] The third mass loss at

about 400 °C confirms dehydration of structural water from YOOH phase.[34]

3.2. Morphology Characterization.

The morphology of the as-obtained samples are examined by FESEM. It can be observed in Fig. 4A that the as-prepared Y_2O_3 illustrates a uniform flake-like shape with irregular edges. Its lateral size ranges from 70 to 150 nm and thickness is around 10 to 20 nm. It can be observed that the prepared graphene oxide illustrates the flake-like shape and layer-layer structure of graphene oxide edges (Fig. 4B). Fig. 4C and D displays the morphologies of 5 GOY and 20 GOY composites, respectively. As can be seen, with GO content increasing, the flake-like structure becomes irregular. At the same time GO and Y_2O_3 aggregate. The EDX profile (Fig. 4D insert) exhibits strong carbon, oxygen and yttrium peaks. Fig. 4E and F exhibit HRTEM images of the GOY composite. As shown in Fig. 4E and F, the lattice fringes of Y_2O_3 nanocrystals and GO are simultaneously observed, indicating strong interactions between Y and the GO support. The resolved lattice fringes of (111) planes (d = 0.31 nm) are attributed to GO, and the lattice fringes of (111) planes (d = 0.27 nm) are assigned to Y_2O_3 nanocrystals.

3.3. XPS analysis.

Fig. 5A shows the XPS full survey spectra in the binding energy range of 0-1100 eV for GO, Y_2O_3, 5 GOY and 20 GOY composite. As shown in Fig. 5A, all the samples contain C and O, however, the Y-contained samples show two peaks at about 158.2 eV and 160.0 eV, which are attributed to Y.[6] Fig. 5B-D shows the high-resolution XPS regional spectra of Y 3d, O 1s and C 1s for 5 GOY, respectively. The relatively strong peaks at 158.1 eV and 159.9 eV can be attributed to Y $3d_{5/2}$ and Y $3d_{3/2}$, respectively (Fig. 5B). These results are in agreement with values of Y_2O_3 reported in the literature.[35] It is well reported that yttrium retards the combination of photogenerated electron-hole pairs,[4,17,18] this may be due to the presence of extra hydroxyl species to delay recombination through hole trapping.[6] Three kinds of surface oxygen species could be distinguished in the O 1s spectra, as shown in Fig. 5C. The binding energy of 530.9 eV, 531.8 and 533.0 eV are ascribed to the lattice oxygen, the hydroxyl groups and the C-OH, respectively.[36] As shown in Fig. 5D, the XPS spectrum of C 1s from 5 GOY is collected, which can be deconvoluted into four peaks: sp^2 bonded carbon at 284.8 eV (C–C), epoxy/hydroxyls at 286.0 eV (C–O), carbonyls at 287.9 eV (C=O), and carboxyls at

289.1 eV (O–C=O), indicating the high percentage of oxygen-contained functional groups.[37] Chemisorbed surface hydroxyl groups can enhance photocatalysis by trapping photoinduced holes resulting in an increase in the formation of highly oxidizing ·OH radicals.[38]

3.4. Photocatalytic Activity for dye degradation.

For comparative purposes, the photodegradation efficiencies of MB and MO mediated by the different photocatalysts under UV irradiation are shown in Fig. 6. Before comparison, the adsorption and photodegradation performances of GO, Y_2O_3 and 5 GOY on MB were investigated (Fig. S1). As displayed in Fig. S1, both Y_2O_3 and 5 GOY have good adsorption affinity to MB. After stirring for 30 min under dark, about 80% MB could be absorbed by Y_2O_3 and 5 GOY, which is much better than GO (lower than 20%). After photocatalysis for 35min, MB can be degraded thoroughly by 5 GOY. Then, the photocatalytic activities of the GO, Y_2O_3, 5 GOY, 10 GOY, 20 GOY and 50 GOY composite photocatalysts were compared via the reduction of MB and MO under ambient temperature. Photodegradation time is 35 min. It has been reported that a large surface area helps to increase the photocatalytic reaction sites.[39] From the O1s spectrum of Y_2O_3 (Fig. S2, supplementary material), the oxygen composition of Y_2O_3 and 5 GOY samples at different states (Table S1, supplementary material), more ·OH radicals are available in 5 GOY. As expected, under UV irradiation the degradation of MB is slower than 10% with a GO photocatalyst. However, the conversion of MB reaches 95% after 35 min when using Y_2O_3 as a photocatalyst. The four kinds of GOY samples exhibite better photocatalytic properties in the degradation of MB than bare GO and Y_2O_3 under UV irradiation. Moreover, with increasing the amount of GO, the degradation of MB increases slowly. Considering the simplicity and economy of the MB degradation, 5 GOY is selected as the photocatalyst in the following experiments. The photocatalytic activities of 5 GOY was compared with commercial TiO_2 P25 (Fig. S3, supplementary material), indicating the photocatalytic property of 5 GOY was quite comparable with P25. The GOY composites also have photocatalytic activities to MO. As can be seen in Fig. 6, GO has good affinity to MO and the 50 GOY has best degradation efficiency to MO among the GOY composites.

The photocatalyst dosage may affect the MB degradation efficiency. Fig. 7A illustrates MB degradation at varying photocatalyst dosages (5 to 10 mg). MB degradation efficiency

increases with increasing the contact time. In addition, with increasing the dosage, the MB degradation efficiency slowly increases. As displayed in Fig. 7A, the best dosage is 10 mg.

As the MB concentration may also influence degradation, MB degradation under various concentration of MB is investigated. It can be seen clearly in Fig. 7B that MB conversion efficiency is as much as 100% after degradation for 35 min when the MB concentration is lower than 25 mg L^{-1}. The conversion efficiency will decrease when the MB concentration is higher than 27.5 mg L^{-1}. The final conversion efficiency will no more than 90% if 30.0 mg L^{-1} MB solution is used.

Because the solution pH can remarkably influence MB degradation, the effect of initial pH on the degradation of MB with 5 GOY catalyst is determined as presented in Fig. 7C. As shown in Fig. 7C, the conversion of MB will finally reach 100% when the solution pH is lower than 5.19. If the solution pH controlled at 6.3, the conversion efficiency will decrease sharply and only 80% MB will convert after 35 min. Therefore, the solution pH is set at 4.1.

3.5. Photocatalytic mechanism

The magnitude of the photocurrent represents the charge collection efficiency of the electrode surface, and indirectly indicates the separated efficiency of electron-hole pairs.[40] From the insert of Fig. 8, 5 GOY modified photoelectrode is prompted in generating photocurrent under visible and UV-visible light. GOY photoelectrodes yield the greater photocurrent than Y_2O_3 photoelectrode under UV irradiation in Fig. 8.

Fig. 9 shows the PL spectra of the Y_2O_3 and GOY photocatalysts. With Y_2O_3 as photocatalyst, the PL signal centered around 450 nm is detected, revealing that ·OH radicals are generated on the irradiated Y_2O_3. When GOY nanocomposites are used as the photocatalysts, the PL signal intensity is increased, which suggests that the yield of ·OH radicals is enhanced on the irradiated GOY nanocomposite. The enhancement in photoactivity can be attributed to the remarkable synergistic effect of the combination of Y_2O_3 and the GO sheets, leading to the efficient separation of photogenerated carriers in the Y_2O_3 and GO coupling system.

It is well known that the photodegradation process of the photocatalysts is strongly relative to electron-hole pairs generated by light irradiation on catalysts. The photogenerated electrons and holes can migrate to the surface of the catalysts and then can be trapped,

generally by the oxygen and surface hydroxyls, to ultimately produce hydroxyl radicals (·OH) that react with the adsorbed reactants.[41] As we know, Y_2O_3 is n-type semiconductor with a wide band gap about 5.6 eV.[42] To understand the charge separation process of Y_2O_3 and GOYs, the band edge positions of conduction band (CB) and valence band (VB) of semiconductor Y_2O_3 has been calculated by the following equation:[43]

$$E_{VB} = X - E^e + 0.5E_g \quad (1)$$

$$E_{CB} = E_{VB} - E_g \quad (2)$$

where X is the absolute electronegativity of the semiconductor, E^e is the energy of free electrons on the hydrogen scale (~4.5 eV), and E_g is the bandgap energy of the semiconductor. The value of X for Y_2O_3 is obtained, by the arithmetic mean of the electron affinity and the first ionization of the constituent atoms reported in the literatures,[44] to be 5.35 eV. Thus, the CB and VB potentials of Y_2O_3 are calculated to be -1.95 and 3.65 eV versus normal hydrogen electrode (NHE), respectively. It can be seen that the VB potential of sample is more positive than the redox potential of OH^-/·OH (1.89 V/NHE), indicating that the photogenerated holes have strong oxidative ability and they can oxidize OH^- into ·OH. In addition, the CB potential of sample is negative enough to reduce O_2 to $O_2^{\cdot -}$ (−0.13 V/NHE) via e^-.

Based on these results, a possible mechanism for the photocatalytic is proposed as follows and shown in Fig. 10.

$$Y_2O_3 + h\nu \rightarrow Y_2O_3\,(h+e) \quad (3)$$

$$Y_2O_3\,(e) + GO \rightarrow Y_2O_3 + GO\,(e) \quad (4)$$

$$GO\,(e) + O_2 \rightarrow GO + O_2^{\bullet -} \quad (5)$$

$$Y_2O_3\,(h) + OH^- \rightarrow Y_2O_3 + OH^{\bullet} \quad (6)$$

$$Y_2O_3\,(h) + O_2^{\bullet -} + OH^{\bullet} + MB \rightarrow CO_2 + H_2O + SO_4^{2-} + NO_3^- + Cl^- \quad (7)$$

4. Conclusions

In conclusion, a novel GOY nanocomposite with different GO content has been obtained via a one-step hydrothermal method. The FT-IR, XRD, EDX and XPS results showed the yttrium was successfully composited with GO. The morphology characterization showed the as-obtained GOY had nanoflake structure. After stirring for 30 min under dark, about 80%

MB could be absorbed by Y_2O_3 and 5 GOY. The as-prepared GOY had good degradation performance on both MB and MO under UV irradiation. Compared with other GOY composites, 5 GOY had better photocatalytic activity to MB. Factors, such as dosages of photocatalyst, contaminant concentration and solution pH on MB conversion were also investigated and discussed. The catalyst also showed good stability and recyclability. It is expected that the GOY nanocomposite would be a potential candidate for treatment of dye containing wastewater.

Acknowledgments

This work was supported by the National Natural Science Foundation of China (No. 21307104), Natural Science Foundation of Jiangsu Province, China (No.BK20130438), the Scientific Research Project of Environmental Fund of Yangzhou City (YHK1303) and Jiangsu Key Laboratory of Environmental Material and Engineering (K12031). We thank the Testing Center of Yangzhou University for sample characterization.

Notes and References

1 B. K. Korbahti, K. Artut, C. Gecgel, A. Ozer, *Chem. Eng. J.*, 2011, **173**, 677-688.

2 V. K. Gupta, D. Pathania, S. Agarwal, P. Singh, *J. Hazard. Mater.*, 2012, **243**, 179-186.

3 N. Wetchakun, S. Chaiwichain, B. Inceesungvorn, K. Pingmuang, S. Phanichphant, A. I. Minett, J. Chen, *ACS Appl. Mater. Interfaces*, 2012, **4**, 3718-3723.

4 Y. F. Li, D. Xu, J. I. Oh, W. Shen, X. Li, Y. Yu, *ACS Catal.*, 2012, **2**, 391-398.

5 M. Khan, W. B. Cao, *J. Mol. Catal. A: Chem.*, 2013, **376**, 71-77.

6 Y. F. Wu, Q. J. Zhang, X. F. Yin, H. Q. Cheng, *RSC Advances*, 2013, **3**, 9670-9676.

7 F. H. Chu, C. W. Huang, C. L. Hsin, C. W. Wang, S. Y. Yu, P. H. Yeh, W. W. Wu, *Nanoscale*, 2012, **4**, 1471-1475.

8 L. J. Xu, J. L. Wang, *Environ. Sci. Technol.*, 2012, **46**, 10145-10153.

9 Y. C. Zhang, J. Li, H. Y. Xu, *Appl. Catal. B*, 2012, **123-124**, 18-26.

10 S. Usai, S. Obregón, A. I. Becerro, G. Colón, *J. Phys. Chem. C*, 2013, **117**, 24479-24484.

11 A. K. Geim, K. S. Novoselov, *Nat. Mater.*, 2007, **6**, 183-191.

12 K.-Y. Shin, J.-Y. Hong, J. Jang, *Adv. Mater.*, 2011, **23**, 2113-2118.

13 G. K. Pradhan, D. K. Padhi, K. M. Parida, *ACS Appl. Mater. Interfaces*, 2013, **5**, 9101-9110.

14 E. Lee, J. Y. Hong, H. Kang, J. Jang, *J. Hazard. Mater.*, 2012, **219-220**, 13-18.

15 Y. S. Fu, H. Q. Chen, X .Q. Sun, X. Wang, *Appl. Catal. B*, 2012, **111-112**, 280-287.

16 K. Krishnamoorthy, R. Mohan, S. J. Kim, *Appl. Phys. Lett.*, 2011, **98**, 244101.

17 M. Li, J. Zhang, Y. Zhang, *Chem. Phys. Lett.*, 2012, **527**, 63-66.

18 F. Meng, J. Li, Z. Hong, M. Zhi, A. Sakla, C. Xiang, N. Wu, *Catal. Today*, 2013, **199** 48-52.

19 H. Zhang, K. Tan, H. Zheng, Y. Gu, W. F. Zhang, *Mater. Chem. Phys.*, 2011, ***125***, 156-160.

20 X. Niu, S. Li, H. Chu, J. Zhou, *J. Rare Earths*, 2011, **29**, 225-229.

21 H. Narayan, H. Alemu, L. Setofolo, L. Macheli, *ISRN Phys. Chem.* 2012, **841521**, 1-9.

22 M. J. Allen, V. C. Tung, R. B. Kaner, *Chem. Rev.*, 2010, **110**, 132-145.

23 F. Y. Ban, S. R. Majid, N. M. Huang, H. N. Lim, *Int. J. Electrochem. Sci.*, 2012, **7**, 4345-4351.

24 Y. L. Min, G. Q. He, Q. J. Xu, Y. C. Chen, *J. Mater. Chem. A*, 2014, **2**, 1294-1301.

25 W. Fan, W. Gao, C. Zhang, W. W. Tjiu, J. S. Pan, T. X. Liu, *J. Mater. Chem.*, 2012, **22**, 25108-25115.

26 Z. -S. Wu, W. Ren, L. Wen, L. Gao, J. Zhao, Z. Chen, G. Zhou, F. Li, H. -M. Cheng, *ACS Nano*, 2010, **4**, 3187-3194.

27 J. A. Dorman, Y. B. Mao, J. R. Bargar, J. P. Chang, *J. Phys. Chem. C*, 2010, **114**, 17422-17427.

28 R. P. Ermakov, V.V. Voronov, P. P. Fedorov, *Nanosystems: physics, chemistry, mathematics*, 2013, **4 (2)**, 196-205.

29 A. Lerf, H. He, M. Forster, J. Klinowski, *J. Phys. Chem. B*, 1998,**102(23)**, 4477-4482.

30 G. Wang, Z. Yang, X. Li, C. Li. *Carbon*, 2005, **43(12)**, 2564-2570.

31 S. Stankovich, D. A. Dikin, R. D. Piner, K. A. Kohlhaas, A. Kleinhammes, Y. Y. Jia, Y. Wu, S. T. Nguyen, R. S. Ruoff, *Carbon*, 2007, **45**, 1558-1565.

32 M. Aghazadeh, A. Nozad, H. Adelkhani, M. Ghaemi, *J. Electrochem. Soc.*, 2010, 157, D519-D522.

33 L. Nan, Y. Kazumichi, *J. Solid State Chem.*, 2008, **181**, 1738-1743.

34 R. Srinivasan, N. R. Yogamalar, J. Elanchezhiyan, R. J. Joseyphus, A. C. Bose, *J. Alloy. Compd*, 2010, **496**, 472-477.

35 S. Somacescu, J. M. C. Moreno, P. Osiceanu, B. L. Su, V. Parvulescu, *J. Phys. Chem. C*, 2010, **114**, 19365.

36 J. H. Pan, W. I. Lee, *Chem. Mater.*, 2006, **18**, 847-853.

37 Y. Chen, B. H. Song, X. S. Tang, L. Lu, J. M. Xue, *J. Mater. Chem.*, 2012, **22**, 17656-17662.

38 J. Xu, Y. Chang, Y. Zhang, S. Ma, Y. Qu, C. Xu, *Appl. Surf. Sci.*, 2008, **255**, 1996-1999.

39 L.P. Zhu, N.C. Bing, L.L. Wang, H.Y. Jin, G.H. Liao, L.J. Wang, *Dalton Trans.*, 2012, **41**, 2959-2965.

40. Z. Pei, L. Ding, H. Lin, S. Weng, Z. Zheng, Y. Hou, P. Liu, *J. Mater. Chem. A*, 2013, **1**, 10099-10102.

41.Y. L. Pan, S. Z. Deng, L. Polavarapu, N. Y. Gao, P. Y. Yuan, C. H. Sow, Q. H. Xu, *Langmuir*, 2012, **28**, 12304-12310.

42. P. Rouffignac, J. S. Park, R. G. Gordon, *Chem. Mater.* 2005, **17**, 4808-4814.

43. H. Xu, H. Li, C. Wu, J. Chu, Y. Yan, H. Shu, Z. Gu, *J. Hazard. Mater*., 2008, **153**, 877-880.

44. T. Andersen, H. K. Haugen, H. Hotop, *J. Phys. Chem. Ref. Data*, 1999, **28(6)**, 1511-1533.

Figure captions

Figure 1. FT-IR spectra of GO, Y_2O_3, and 5 GOY composites.

Figure 2. XRD patterns of GO, Y_2O_3 and 5 GOY composites.

Figure 3. TGA curves of GO, Y_2O_3 and 5 GOY composites.

Figure 4. FESEM images of (A) Y_2O_3 (Insert: low magnification), (B) GO, (C) 5 GOY and (D) 20 GOY composites (Insert: EDS spectrum of 20 GOY sample); (E) and (F) HRTEM images of 5 GOY taken after intense ultrasonic dispersion in ethanol for 30 min.

Figure 5. XPS spectra. (A) full survey spectra of GO, Y_2O_3 and GOY nanocomposite, (B) Y 3d of 5 GOY, (C) O 1s of 5 GOY, (D) C 1s of 5 GOY.

Figure 6. Comparison of photodegradation efficiency using as-synthesized GO, Y_2O_3 and GOY composites.

Figure 7. (A) Effect of dosage on MB conversion. MB concentration: 25 ppm, pH = 4.1. (B) Effect of MB concentration on the degradation. Dosage: 10 mg, pH = 4.1. (C) Effect of solution pH on MB conversion. MB concentration: 25 ppm. Dosage: 10 mg.

Figure 8. Photocurrent responses of GO, Y_2O_3 and 5 GOY photoelectrodes under UV illumination. Insert: Photocurrent responses of 5 GOY under different illumination conditions. Scan rate: 50 mV/s. The electrolyte solution was 0.5 M NaCl.

Figure 9. PL spectra of Y_2O_3, 5 GOY and 20 GOY samples (λex = 258 nm).

Figure 10. Proposed mechanism for the photodegradation of MB on GOY composite.

Figure 1

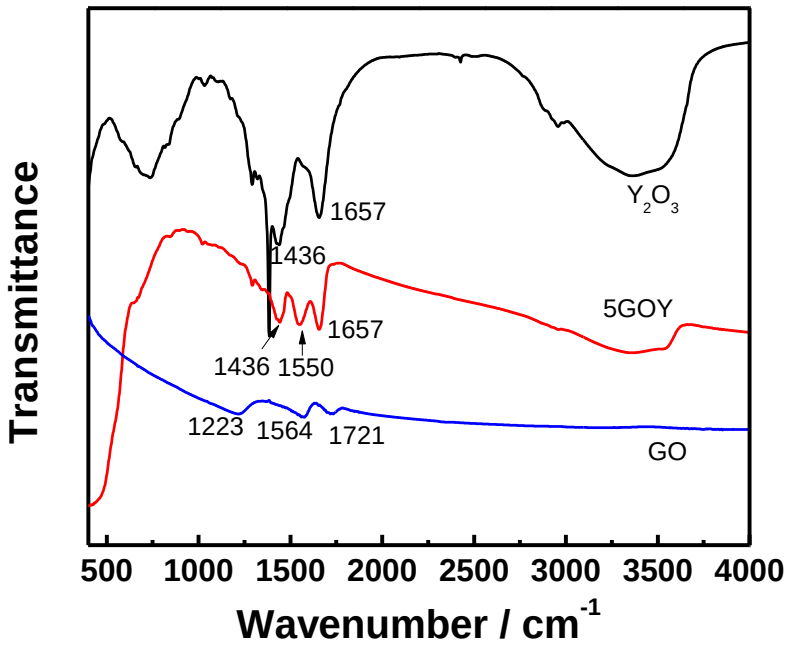

Figure 2

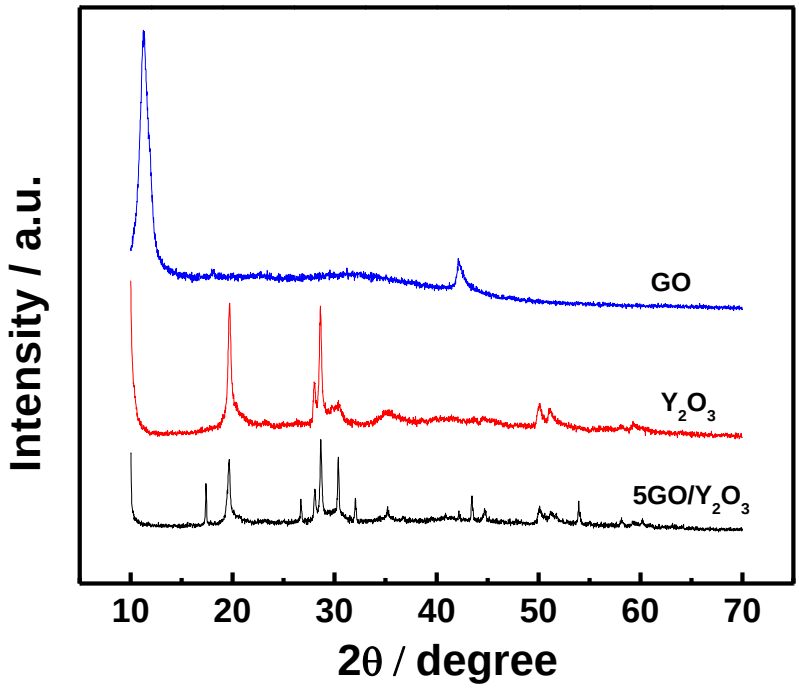

1 Figure 3
2

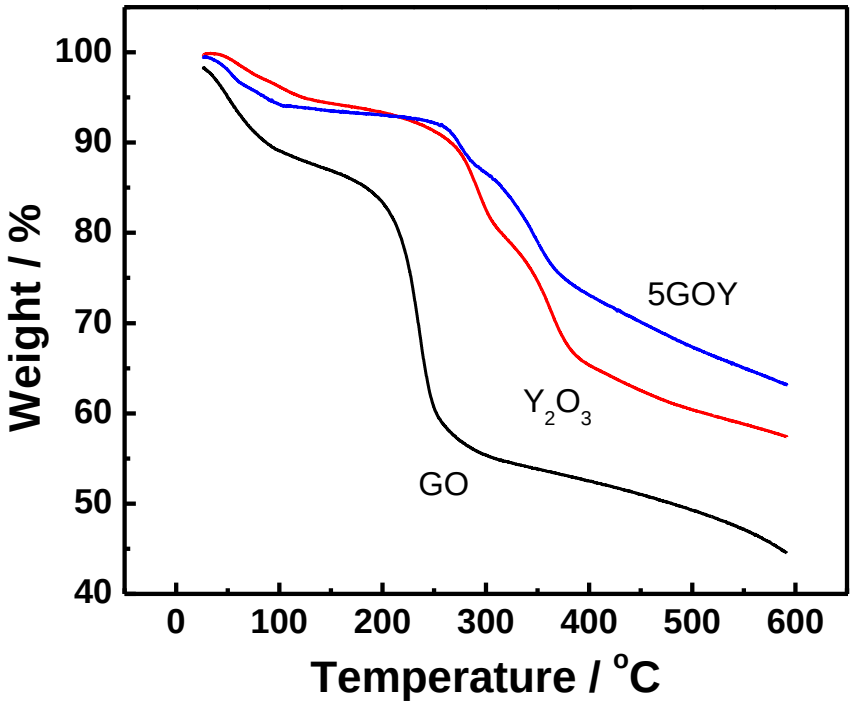

3
4

Figure 4

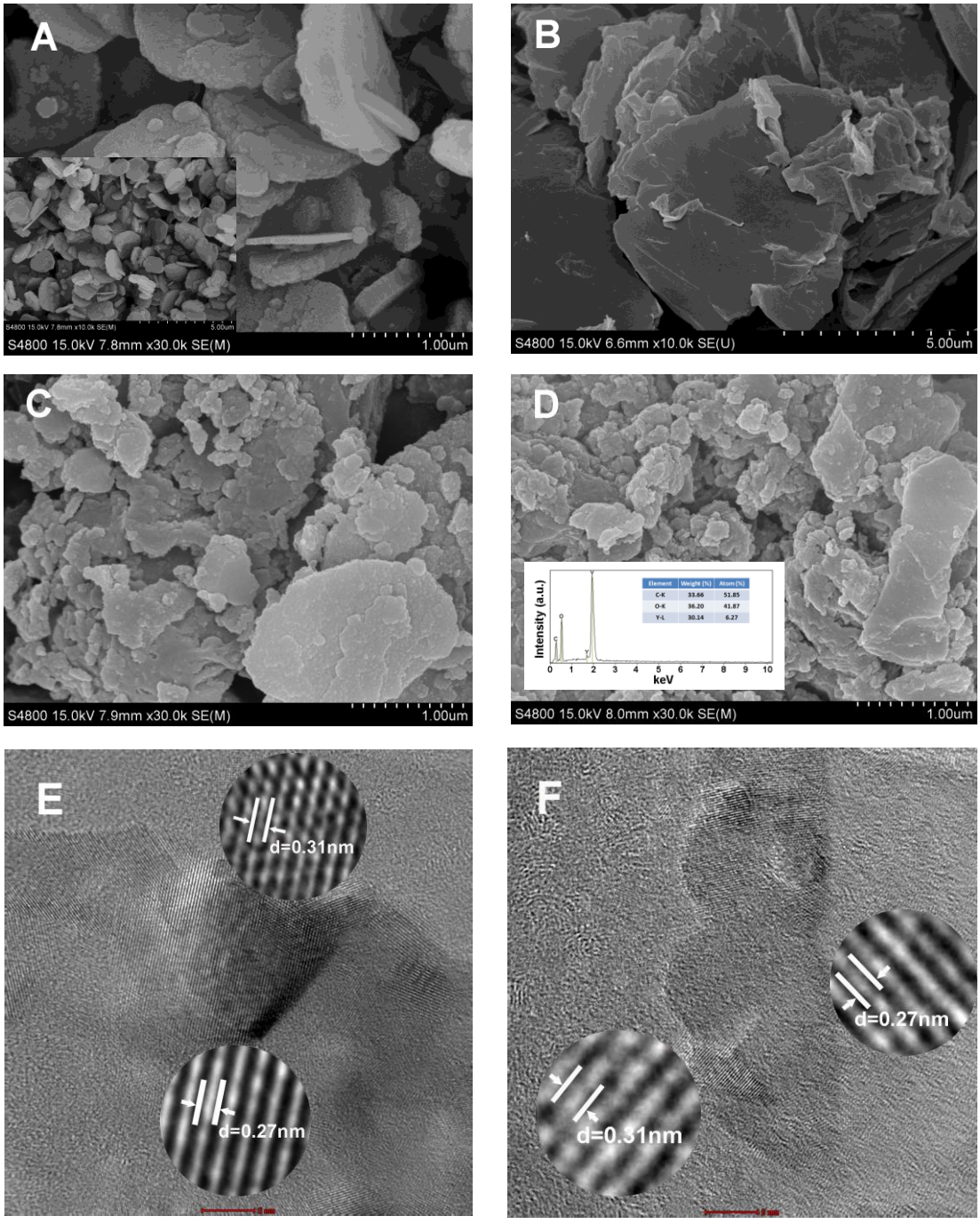

Figure 5

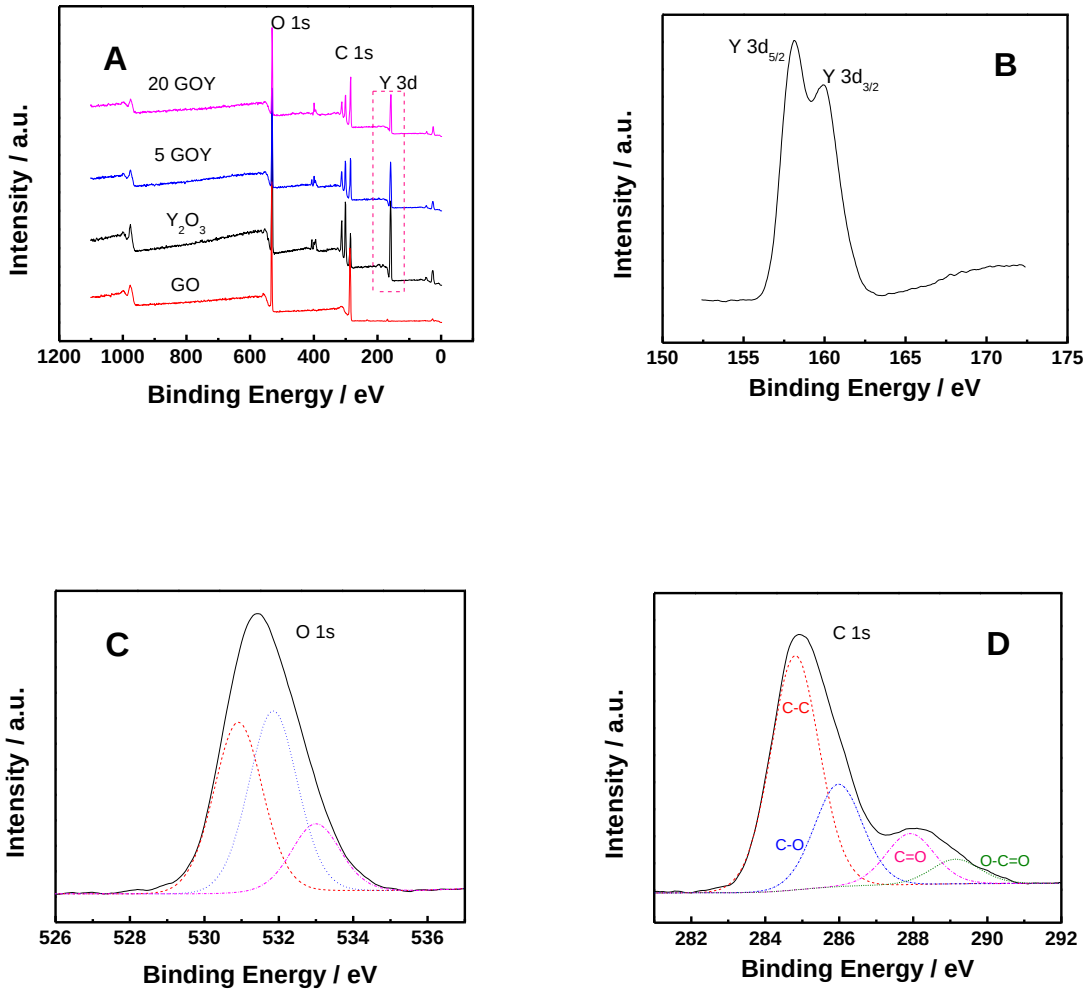

Figure 6

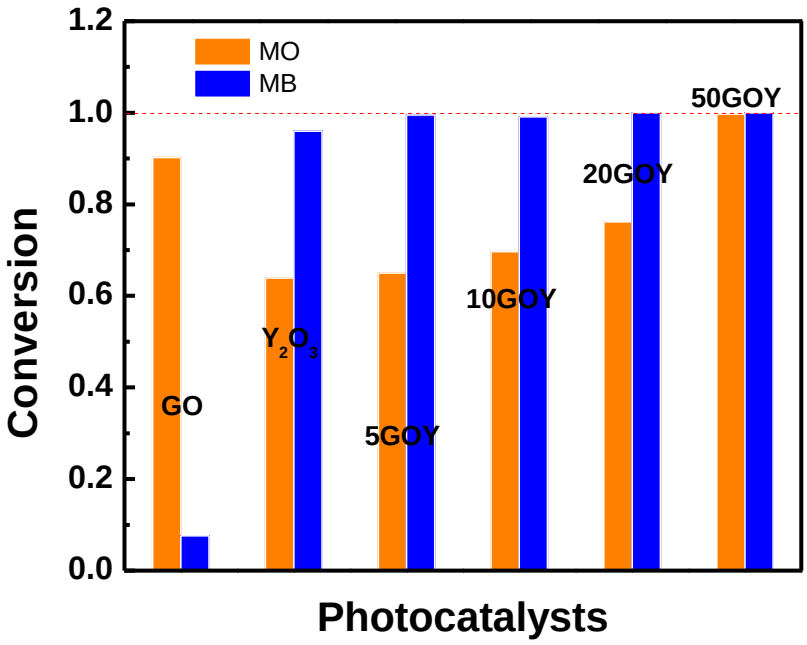

Figure 7

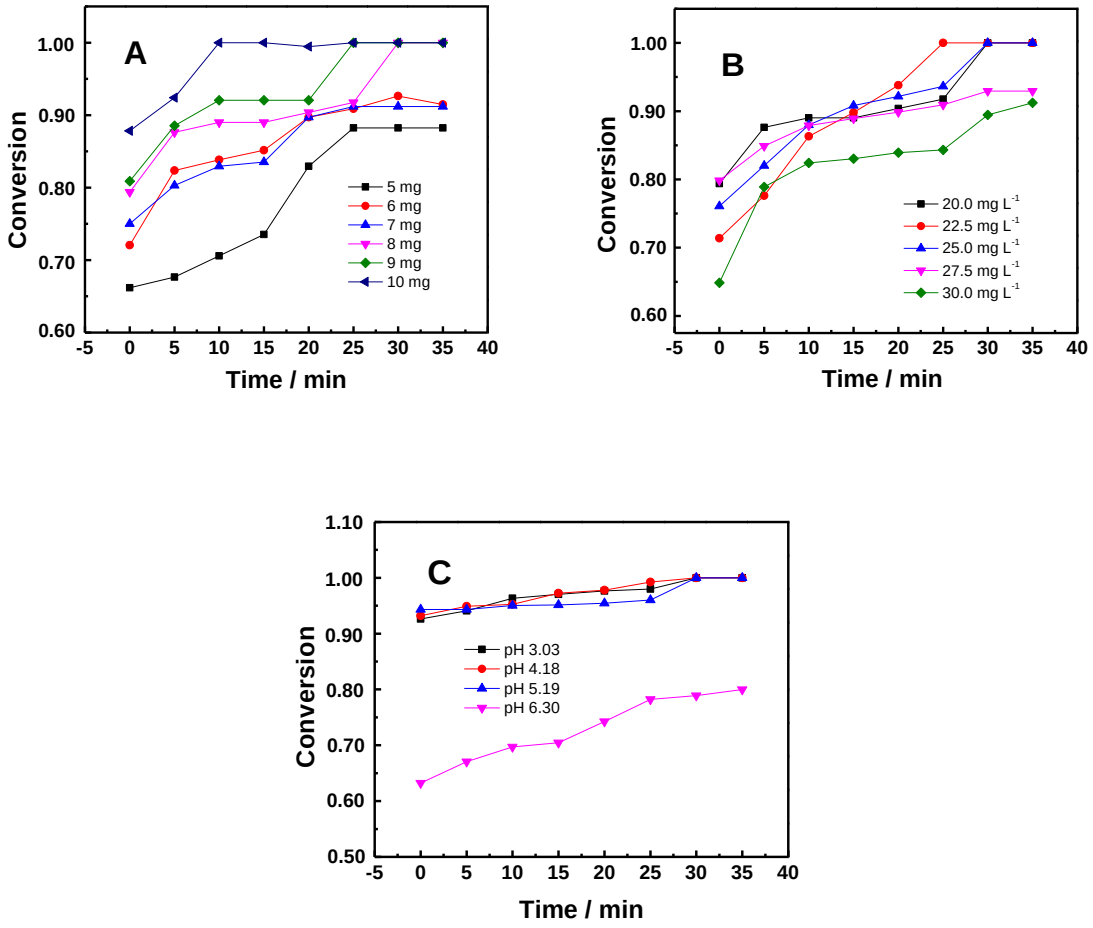

Figure 8

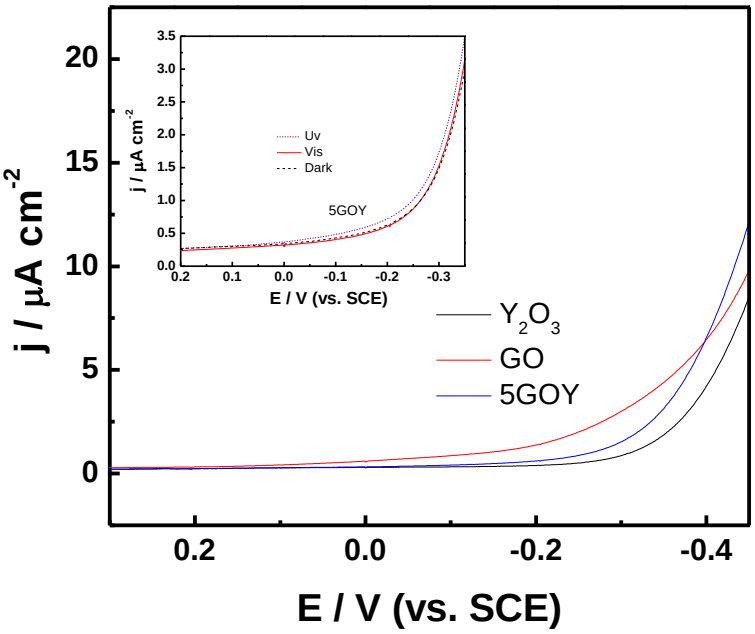

Figure 9

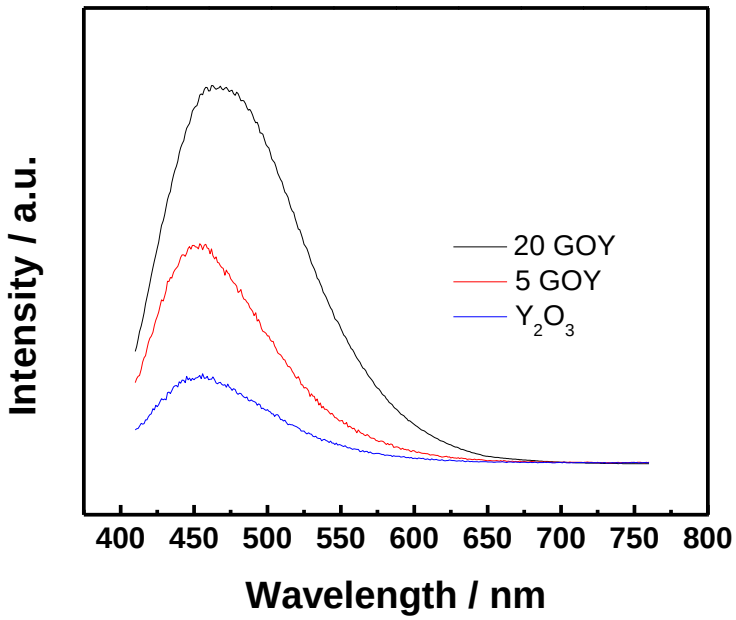

Figure 10